Direct Measurements of Single-Event Burnout Current Induced by Neutron Irradiation in a 1200 V Fast Recovery Diode

Hikaru Nakamoto, *Graduate Student Member, IEEE*, Jun Furuta, *Member, IEEE*, Vanness Filbert Cierra, Yoshinari Kamakura, *Member, IEEE*, Michitarou Yabuuchi, Hironori Sakamoto, Ryuichi Nakajima, *Graduate Student Member, IEEE*, Shuhei Mandai, Kazutoshi Kobayashi, *Senior Member, IEEE*, Makoto Sakai, *Member, IEEE*, and Shigetaka Kumashiro, *Life Senior Member, IEEE*

***Abstract*—This work investigates Single Event Burnout (SEB) in a 1200 V Si Fast Recovery Diode (FRD) through neutron irradiation experiments and device simulations. Transient current and voltage measurements revealed that SEB is not determined by the initial current peak alone but evolves into a destructive state through subsequent carrier multiplication via impact ionization. Statistical measurements at 930 V without parallel capacitance showed that only one in ten irradiation events led to burnout, providing direct experimental evidence that SEB initiation is governed by stochastic upward fluctuations in impact ionization rather than by a deterministic threshold. Cross-sectional analyses provides a quantitative comparison of damage patterns under different parallel capacitances. To reproduce the experimental measurements in device simulations, worst-case secondary-ion conditions were extracted using the Particle and Heavy Ion Transport code System (PHITS) and applied in TCAD. Default TCAD with the van Overstraeten-de Man avalanche model underestimated both the peak and persistence of SEB currents. However, by modifying the avalanche parameter so that the ionization coefficient is evaluated at an effective electric field 1.41 times larger than usual, and by applying a linear energy transfer (LET) multiplier of 30 to compensate for the missing carrier formation energy, the simulated current quantitatively matched the measured sharp rise and sustained current growth. While fully quantifying the exact factor of 30 remains a subject for future work, the issue of initial energy is considered one of the potential factors necessitating this large scaling to phenomenologically compensate for standard TCAD limitations. These results provide a quantitative reproduction of SEB current under neutron irradiation and establish a practical framework for understanding the stochastic nature of burnout.**

***Index Terms*—Single-Event Burnout (SEB), Fast Recovery Diode (FRD), Impact ionization, device simulation, Monte Carlo simulation, neutron irradiation, clinical carbon beam.**

I. Introduction

H. Nakamoto, R. Nakajima, S. Mandai, and K. Kobayashi are with the Graduate School of Science & Technology, Kyoto Institute of Technology, Matsugasaki, Sakyo-ku, Kyoto 606-8585, Japan (e-mail: hnakamoto@vlsi.es.kit.ac.jp).

J. Furuta is with the Department of Information and Communication Engineering, Okayama Prefectural University, Okayama 719-1197, Japan.

V. F. Cierra and Y. Kamakura are with the Department of Information and Computer Science, Osaka Institute of Technology, Osaka 573-0196, Japan.

M. Yabuuchi, H. Sakamoto, and S. Kumashiro are with Renesas Electronics Corporation, Tokyo 187-8588, Japan.

M. Sakai is with the Gunma University Heavy Ion Medical Center (GHMC), Gunma 371-8511, Japan, and also with the Graduate School of Medical Sciences, Kyushu University, Fukuoka 812-8582, Japan.

HIGH reliability is essential for power semiconductors in advanced industrial applications. However, some devices are highly susceptible to radiation-induced destructive failures, requiring radiation-resistant designs. Single Event Burnout (SEB) occurs when a radiation particle strikes a device in the off state, generating electron-hole pairs. This leads to a localized current increase due to impact ionization, ultimately causing unrecoverable permanent failure. Thus, improving SEB resistance is crucial.

In previous SEB studies, current and voltage transients under irradiation have been reported [1]–[4]. However, these measurements were generally limited to relatively coarse temporal resolution, insufficient to resolve the nanosecond-scale dynamics governing SEB initiation and its evolution into destructive burnout [5]. Most prior measurement works were focused on failure occurrence rates or cross-sectional analyses of damage regions, leaving the direct correspondence between transient current evolution and irreversible device failure unexplored. As a result, the early stages of current growth leading to SEB have remained experimentally unclear. In this study, we specifically address this issue by undertaking high-resolution measurements of SEB current and voltage waveforms under neutron irradiation, capturing the rapid transient processes that have not been experimentally accessible before.

Alongside experimental efforts, device-level simulations using TCAD have been widely applied to analyze SEB mechanisms [6], [7]. These simulations provide detailed insights into internal electric fields, carrier dynamics, and avalanche multiplication processes that cannot be directly observed in experiments. However, most reported TCAD studies have been performed without direct comparison to experimentally measured SEB current. In many cases, simulation parameters have been adjusted to reproduce failure occurrence qualitatively, but their quantitative validity has remained uncertain [8]. This lack of validation poses a major limitation. Without experimental current waveform data to serve as benchmarks, it is impossible to assess whether TCAD results accurately capture the magnitude, time scale, and persistence of SEB currents. A rigorous, side-by-side comparison between measured SEB currents and device simulations is therefore essential to establish the credibility of TCAD-based interpretations. In this study, we explicitly address this issue by performing a direct

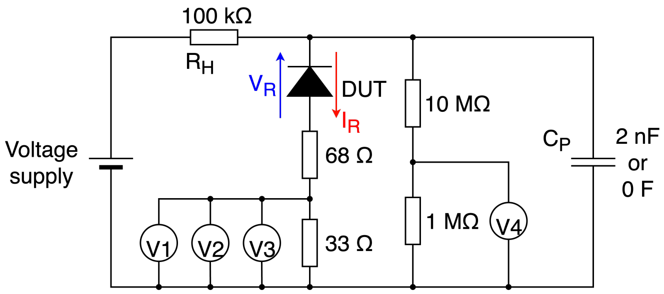

Fig. 1. Measurement circuit for SEB characterization. V1, V2, and V3 denote current probes with different sensitivities, and V4 monitors the applied reverse voltage V_{R}.

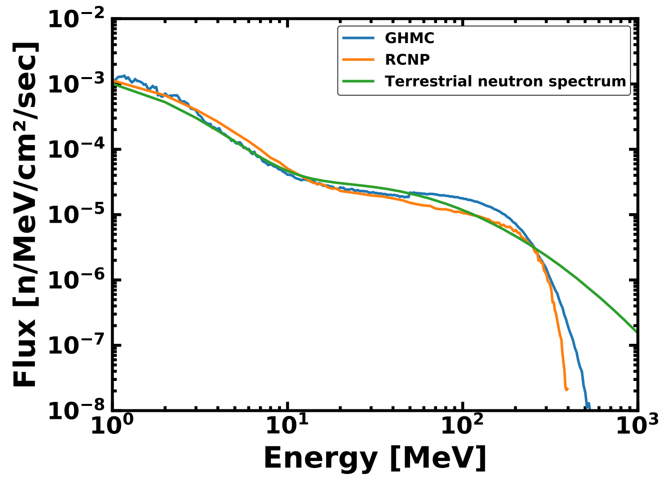

Fig. 2. Neutron energy spectrum at the DUT installation site for RCNP, GHMC, and terrestrial environments, calculated by PHITS. The spectra are normalized by the number of neutrons above $1\ \mathrm{MeV}$ and protons above $50\ \mathrm{MeV}$.

comparison between measured SEB current under neutron irradiation and TCAD device simulations.

Previous TCAD studies have confirmed that impact ionization is indispensable for SEB initiation, as simulations without avalanche models fail to reproduce breakdown [6], [9], [10]. However, these approaches are inherently deterministic and treat impact ionization as a smooth, averaged process. SEB has been observed only in a small fraction of irradiation events under identical conditions, confirming its rare nature [11]. This observation suggests that random fluctuations in impact ionization may influence whether the transient current evolves into destructive burnout. However, the connection between such microscopic variations and the diversity of SEB current waveforms remains unclear. In this study, we address this issue by combining high-resolution experimental waveforms with advanced device simulations, thereby providing new evidence that stochastic variations in impact ionization play a critical role in determining SEB occurrence.

Cross-sectional physical analyses have also been extensively conducted to study SEB-induced damage regions [12]–[14]. Cross-sectional imaging techniques such as electron microscopy have revealed characteristic features, including silicon melting. However, most of these studies treated the observed damage qualitatively, without systematic correlation to the circuit environment during irradiation. In particular, the influence of circuit parameters, such as parallel capacitance, on the extent and severity of damage has not been quantitatively addressed. Since parasitic capacitances are inevitable in practical power circuits, clarifying how stored charge modifies the size and morphology of the damaged region is essential for bridging device-level SEB mechanisms with application-level reliability. In this study, we directly evaluated observed damaged regions under the different parallel capacitance, thereby highlighting the correlation between the parallel capacitance and physical failure.

The rest of this paper is organized as follows. Section II describes the measurement setups. Section III presents the measurement results. Section IV provides a detailed discussion. Section V concludes the paper.

II. Measurement Setups

A. Measurement Circuit

The measurement circuit used for SEB characterization is illustrated in Fig. 1. A 1200 V-rated Si Fast Recovery Diode (FRD) was used as the device under test (DUT). FRD consists of a simple verical p-n^{-}-n diode structure with a p-type anode, a lightly doped n^{-} drift layer designed to sustain the high reverse blocking voltage, and a heavily doped n-type cathode. FRD was evaluated under reverse bias so that the influence of forward-injected carriers is eliminated; the measurements therefore focus purely on the carrier-multiplication dynamics induced by secondary ions [15]. Various reverse voltages V_{R} were applied using the voltage supply through the large series resistance R_{H}, which limits the supply current and ensures that the measured current originates primarily from the ion-induced transient rather than from the power source [16]. Since parallel capacitance plays a significant role in SEB occurrence [17], the parallel capacitor C_{P} was connected across the DUT to investigate the role of stored charge. These two cases were specifically tested: without any additional capacitance ($C_{\mathrm{P}} = 0\ \mathrm{F}$) and with moderate capacitance ($C_{\mathrm{P}} = 2\ \mathrm{nF}$). These values were chosen to assess the extent to which parallel capacitance modifies the SEB onset conditions and the severity of the subsequent avalanche. The SEB current I_{R} was monitored with three current probes (V1, V2, and V3) of different sensitivity to cover a wide dynamic range, while the reverse voltage V_{R} across the DUT was simultaneously measured by the probe V4 to capture the voltage collapse accompanying SEB. All signals were recorded with a high-bandwidth, high-sampling-rate, oscilloscope (DPO7054C, Tektronix) to resolve sub-nanosecond to nanosecond transients. All measurements were carried out at room temperature.

B. Experimental Facilities

We conducted neutron irradiation experiments using two complementary facilities: the white neutron beam at the Re-

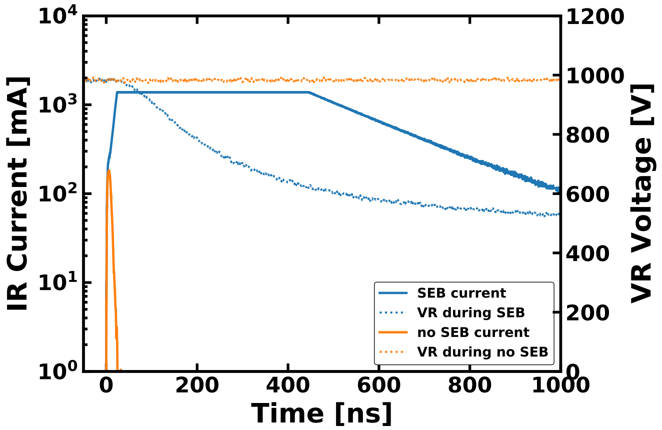

Fig. 3. SEB and non-SEB current waveforms and the SEB-induced voltage drop at $V_R = 980$ V with 2 nF, measured at GHMC. Due to the recording limit, $I_R > 1400$ mA is not captured.

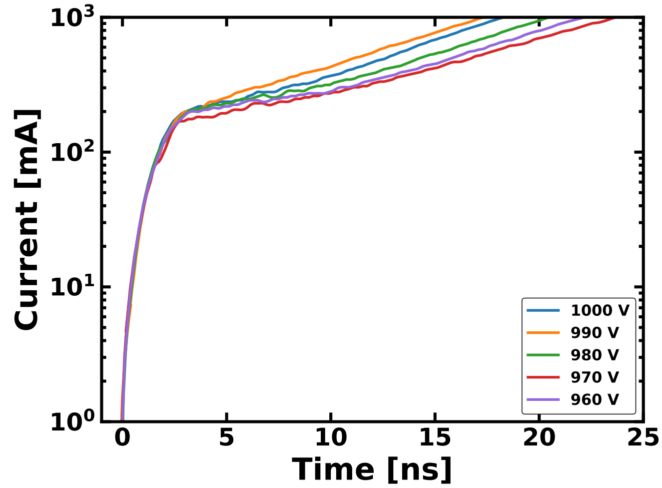

Fig. 4. SEB current during a voltage sweep from $V_R = 960$ V to 1000 V with a parallel capacitance of 2 nF, measured at GHMC.

search Center for Nuclear Physics (RCNP) [18] and the high-energy neutrons generated by a clinical carbon beam at Gunma University Heavy Ion Medical Center (GHMC) [19]. At RCNP, neutrons are produced by irradiating a thick tungsten target with 392 MeV protons, yielding a continuous white neutron spectrum extending up to several hundred MeV. The DUT was placed on-axis at a distance of 216 cm from the production target. This geometry provides a well-characterized spectrum and stable neutron flux, allowing systematic evaluation of SEB under controlled conditions. At GHMC, high-energy neutrons are produced by irradiating the acrylic block with a 290 MeV clinical carbon beam. Nuclear spallation reactions inside the block generate secondary particles, including neutrons, protons, and alpha particles near the Bragg peak [20]. The downstream Pb block is installed to remove charged secondaries, ensuring that only neutrons reach the DUT [21]. Similar nuclear reactions also occur for protons above 50 MeV and for neutrons. [22], [23]. As a result, SEB occurs exclusively due to high energy neutrons [12], with negligible contribution from low energy protons and alpha particles. The neutron energy spectrum at the DUT was calculated using the Particle and Heavy Ion Transport code System (PHITS) [24]. Since the DUT location differs from that in [21], the resulting spectrum is not identical. As compared in Fig. 2, the GHMC spectrum resembles those observed at RCNP and in terrestrial environments [23], [25], but it contains a significantly higher fraction of neutrons above 10 MeV. This high-energy content enables shorter measurement times for SEB occurrence.

III. Measurement Results

Fig. 3 compares the SEB and non-SEB current waveforms and the corresponding voltage responses under $V_R = 980$ V with 2 nF parallel capacitance. SEB occurrence is identified by a clear drop in V_R. Due to the oscilloscopes limitation, currents above 1400 mA were not recorded. In the SEB case, The observed decrease in V_R after I_R reaches approximately 1000 mA suggests a significant reduction in the device's internal resistance, likely due to the formation of a localized damage track. While this may indicate the threshold for observable degradation, it should be noted that the actual initiation of microscopic damage could occur at even lower current levels. After this onset, the current gradually decreases over several hundred nanoseconds, while the voltage continuously falls from 1000 V to about 600 V. This synchronized behavior indicates the progressive expansion of the damage region over time. In contrast, in the non-SEB case, I_R rises briefly to a few hundred mA but rapidly decays within about 10 ns, while V_R remains stable at around 1000 V. The initial rise of the current is nearly identical in both cases, but the subsequent evolution diverges. Thus, the initial current alone cannot determine failure. SEB occurs only if the current persists and drives a voltage collapse. Moreover, the SEB current waveform shows a gradual decay of I_R over hundreds of nanoseconds. During this period, the reverse voltage V_R decreases to approximately 600 V, where the electric field is insufficient to maintain additional avalanche multiplication. The observed current tail is therefore attributed to the discharge of carriers generated during the initial avalanche and to resistive conduction through the damaged region once V_R has collapsed. Transient current pulses may occur frequently, but catastrophic failure arises only when the pre-collapse transient achieves sustained impact-ionization growth that collapses V_R and establishes the damaged conduction path.

Fig. 4 shows SEB current measured from $V_R = 960$ V to 1000 V. Up to 2.5 ns, the current rises are nearly identical across all biases. Beyond this point, the increase does not scale monotonically with voltage. Specifically, the order in which the current reached 1000 mA was 990 V first, followed by 1000 V, 980 V, 960 V, and finally 970 V, which is not proportional to the magnitude of the applied bias. It has been well established that SEB depends on both applied voltage and linear energy transfer (LET) [1]. These results provide a concrete example where these two factors compete. In particular, when the voltage sweep range is narrow, the event-to-event fluctuations in the LET of neutron-induced secondary ions dominate over the relatively small differences in electric-

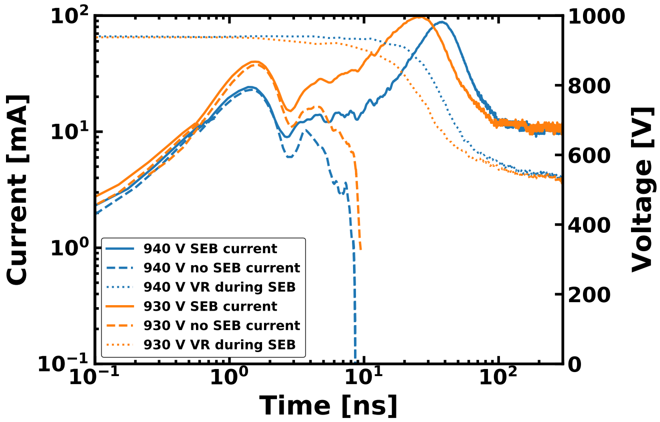

Fig. 5. Representative SEB and non-SEB current waveforms at $V_R = 930$ V and 940 V without parallel capacitance, including both SEB occurrence and non-occurrence cases, along with voltage variation during SEB, measured at RCNP.

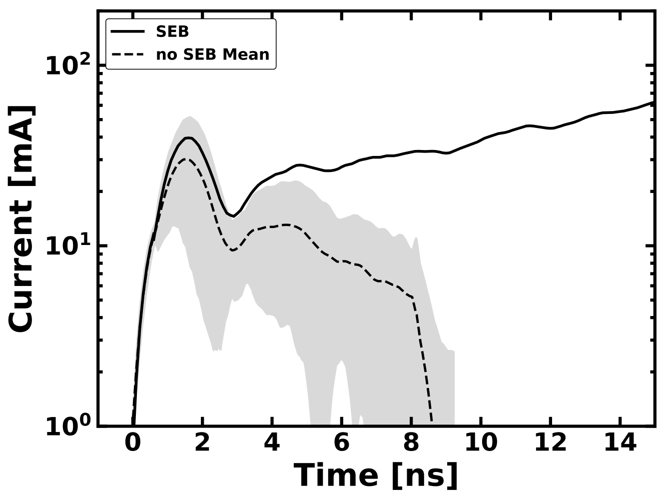

Fig. 6. Statistical variation of current waveforms at $V_R = 930$ V without parallel capacitance. The solid line represents the SEB case, the dashed line shows the mean of nine non-SEB waveforms, and the shaded region indicates their 2σ interval.

field-driven avalanche gain, making the expected voltage dependence less apparent. This highlights the importance of accounting for LET distribution effects when evaluating SEB within a limited voltage range.

Fig. 5 depicts representative SEB current measured at $V_R = 930$ V and 940 V without parallel capacitance. In both cases, the initial current peak around 1.5 ns remained essentially identical regardless of whether SEB occurred, confirming the reproducibility of the initial carrier generation process. However, the SEB waveform shows a distinct behavior after this peak: the current does not simply decay, but instead exhibits repeated fluctuations followed by a gradual increase leading to catastrophic failure. Such non-monotonic behavior suggests a complex interplay between the intrinsically probabilistic and sporadic nature of excessive impact ionization and subsequent local field dynamics, such as temporary field collapsing caused by high carrier densities.

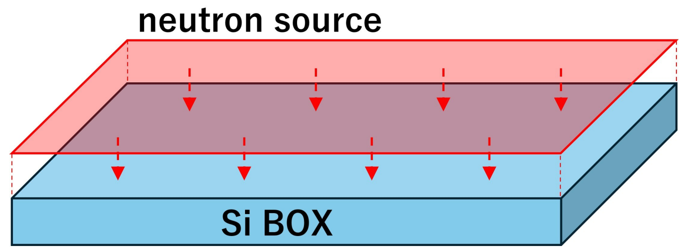

Fig. 7. Simulation geometry in PHITS. A rectangular Si box, whose dimensions reproduce the actual size of the FRD, is irradiated with neutrons using the GHMC spectrum at the DUT location. Secondary ions generated inside Si are recorded to extract their LET and track length.

TABLE I
MAXIMUM LET VALUES AND CORRESPONDING ABSORBED ENERGY METRIC FOR DIFFERENT TRACK LENGTHS OBTAINED FROM PHITS SIMULATIONS

Track Length L [µm] W_{gen} [a.u.]	Maximum LET $\mathrm{LET_{max}}(L)$ [MeV-cm^2/mg]	Absorbed Energy
0.2	1.5	0.3
0.5	7.5	3.75
1	7.5	7.5
4	2.5	10
8	2.5	20
10	2.5	25
20	2.5	50
30	2.5	75
50	0.5	25
80	0.125	10
130	0.125	16.25

Fig. 6 summarizes the statistical variation of the measured current at $V_R = 930$ V without parallel capacitance. Among ten measurements under the same condition, nine cases showed no burnout and one case exhibited SEB, giving an occurrence probability of 10%. The dashed line presents the mean waveform of the nine non-SEB cases, while the shaded region indicates their 2σ interval. The solid line corresponds to the single SEB case. All cases share almost identical initial current peak, confirming the reproducibility of carrier generation. However, only the SEB waveform deviates significantly from the 2σ envelope, exhibiting a delayed avalanche increase that leads to catastrophic failure. These results demonstrate that SEB initiation is not determined solely by a current threshold, but is strongly influenced by stochastic fluctuations in impact ionization.

IV. DISCUSSION

A. SEB Current Reproduction in Device Simulation

For TCAD simulations of SEB, it is essential to specify excitation parameters for a heavy-ion strike, namely the ion LET and the track length. These parameters cannot be obtained directly from neutron irradiation, since only neutrons are incident and the resulting current waveforms do not provide single-event ionization details. Therefore, we used PHITS [24] to evaluate the properties of neutron-induced secondary ions in Si and to extract the most critical ionization conditions. The focus was placed on the worst-case condition, since SEB is a very rare event. Identifying the maximum LET and track

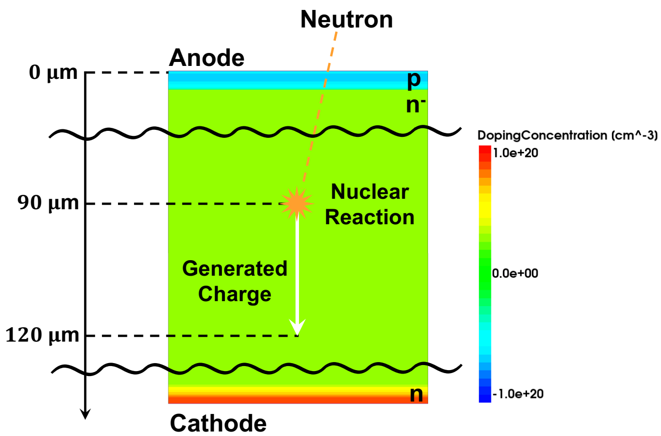

Fig. 8. 2D TCAD cross-sectional view of the simulated 1200 V FRD. The figure illustrates the doping concentration profile, the assumed location of the neutron-induced spallation reaction, and the charge path generated by the resulting secondary ions.

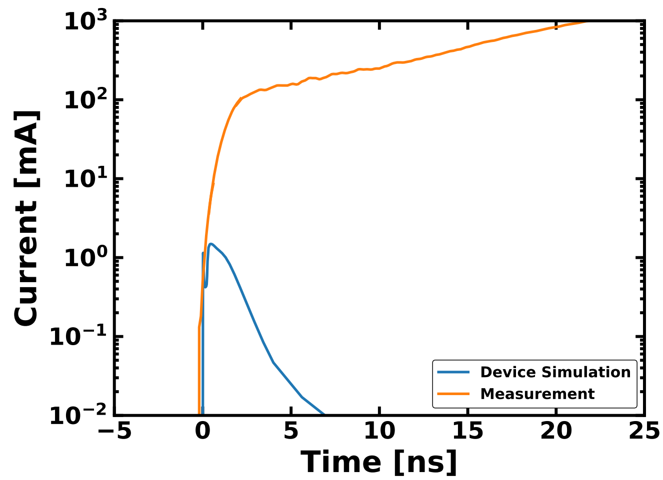

Fig. 9. Comparison between the experimental results and the device simulation with conventional settings. In both experimental and simulation conditions, V_R is set to 1000 V.

length provide an upper-bound source for the parameters of heavy-ion strike models in TCAD. If SEB can be reproduced under this extreme condition, the model is consistent. The procedure was as follows:

1) Geometry and source: A rectangular Si box was irradiated with neutrons using the GHMC spectra at the DUT location (simulation geometry shown in Fig. 7).
2) Tracking: Secondary ions produced in Si were tracked, and their LET and track length were recorded.
3) Absorbed Energy metric: For each track length L, the maximum LET $\mathrm{LET}_{\max}(L)$ was extracted, and the following metric was defined:

$$W_{\mathrm{gen}}(L) = \mathrm{LET}_{\max}(L) \times L. \tag{1}$$

The results are summarized in TABLE I. The largest W_{gen} was obtained from the 30 µm track length and $2.5\ \mathrm{MeV\text{-}cm^2/mg}$ LET, which defines the worst-case condition for SEB initiation. This parameter set was therefore adopted as the heavy-ion input in TCAD simulations to ensure that the simulated conditions faithfully represent the most severe and destructive single event observed under neutron irradiation.

The TCAD simulation was performed using Sentaurus by Synopsys with a three-dimensional device model of the FRD. The model was constructed based on the accurate impurity concentration profiles provided by the manufacturer of the FRD, ensuring a faithful reproduction of the actual device characteristics. Fig. 8 illustrates the 2D cross-sectional view of the simulated 1200 V FRD structure used in the TCAD analysis. The figure visualizes the basic device structure, including the anode/cathode regions and the background doping concentration profile. In this simulation setup, an incident neutron is modeled to strike from the anode side, inducing a nuclear spallation reaction deep within the n^- drift layer. The representative charge path generated by the highly energetic secondary ions is depicted by the solid line, originating from the reaction point and extending toward the cathode. The simulation was carried out under a reverse bias of $V_R = 1000$ V without parallel capacitance ($C_P = 0$ F). To emulate the excitation induced by neutron-generated secondary ions, a heavy-ion strike was injected into the drift region. The parameters of the strike were taken from the worst-case condition identified by PHITS: LET $= 2.5\ \mathrm{MeV\text{-}cm^2/mg}$, track length $= 30$ µm, and a Gaussian temporal profile. The physical models include electric field and doping dependent carrier mobility, along with avalanche generation according to the Chynoweth law [26]. Simulations were performed at room temperature, and thermal effects were neglected.

Fig. 9 compares the measured and simulated results. The experimental waveform exhibits a sharp rise in current within a few nanoseconds, followed by a sustained increase that exceeds hundreds of milliamperes and ultimately leads to destructive burnout. By contrast, the simulated waveform shows only a small transient peak of a few milliamperes, which quickly decays to nearly zero. This stark discrepancy indicates that the simulation severely underestimates both the peak amplitude and the persistence of the SEB current.

SEB cannot be explained by standard avalanche models that describe only average ionization. It is triggered by rare extreme events, and therefore the experimental avalanche current cannot be reproduced by default TCAD models. This indicates that more advanced frameworks are required to capture the phenomenon under neutron irradiation.

However, when the impact ionization model was modified, the agreement with the experimental data significantly improved. In this study, the van Overstraeten-de Man [27] model implemented in Sentaurus was used to describe avalanche ionization,

$$\alpha(F) = \gamma a \exp\left(-\frac{\gamma b}{F}\right), \tag{2}$$

where a and b are empirical fitting parameters and F is the electric field. γ represents the carrier type (electron or hole). To enhance avalanche multiplication, parameter b of Eq. (2) was adjusted so that the ionization coefficient is evaluated at an effective electric field 1.41 times larger than usual. This treatment effectively lowers the critical electric field for impact

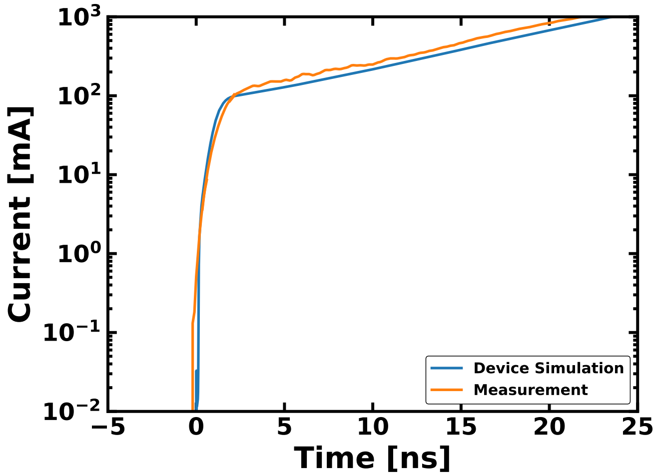

Fig. 10. Comparison between measured SEB current waveform and device simulation at $V_{\mathrm{R}} = 1000$ V. The simulation uses the van Overstraeten-de Man avalanche model with the parameter b adjusted so that the ionization coefficient is evaluated at an effective electric field 1.41 times larger. Heavy ion excitation is defined by a track length of 30 µm and LET of 2.5 MeV-$\mathrm{cm}^2/\mathrm{mg}$, scaled by 30 to represent the worst-case condition from PHITS.

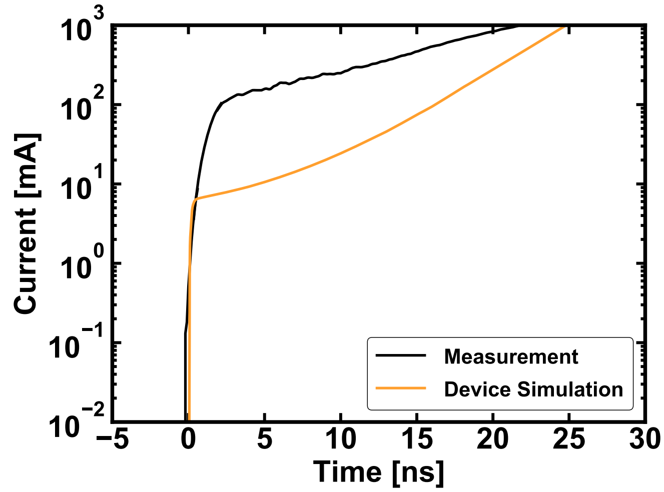

Fig. 11. TCAD simulation result using a standard LET multiplier (1x) and an impact ionization rate increased by a factor of 1.52 (effectively decreasing the critical field). The initial current is significantly underestimated compared to the measurement.

ionization, thereby increasing the probability of avalanche at a given bias. In addition, the initial charge deposition was scaled by an LET multiplier of 30 relative to the worst-case condition extracted from PHITS.

As shown in Fig. 10, the simulation under these adjusted parameters reproduces the experimental current waveform at $V_{\mathrm{R}} = 1000$ V with high fidelity. Both the sharp rise and the sustained growth of the current were captured, in stark contrast to the strong underestimation seen with the default parameter set.

Note that an alternative approach of relying solely on a further decrease of the critical electric field, without applying the LET scaling factor, was also investigated. As demonstrated in Fig. 11, where the effective electric field for evaluating the impact ionization rate was artificially scaled by a factor of 1.52 with a standard 1x LET, this approach fails to reproduce the highly dense initial charge generation required to match the instantaneous current peak observed in the measurement. Furthermore, artificially lowering the critical electric field to the extreme level required to force a match without the LET scaling severely degrades the fundamental static blocking characteristics of the device. The device would become highly susceptible to premature avalanche breakdown even in the absence of an ion strike, making such an approach physically invalid. Therefore, enhancing the localized initial charge generation is a strictly necessary mechanism to accurately reproduce the highly dynamic SEB transient without violating the established baseline physics of the diode.

Furthermore, we investigated how geometric parameters, specifically the strike location and the incident angle of the secondary ions, affect the simulation results. While the strike location primarily shifts the delay time and the initial rising speed due to changes in the carrier transit distance, the incident angle alters the spatial distribution of the initial charge track. However, we confirmed that neither of these geometric variations changes the fundamental necessity for the LET scaling factor and the required impact ionization rates. The requirement to enhance these physical parameters to reproduce the explosive current runaway remains strictly robust, regardless of the specific strike location or incident angle. This confirms that incorporating adjustments to both the ionization model and the excitation strength is essential to reproduce SEB currents.

B. *Influence of Self-Heating Effects*

To validate the isothermal assumption used in our primary analysis, the influence of self-heating on the transient current behavior was rigorously evaluated. Fig. 12 illustrates the simulated transient current and maximum device temperature, comparing the default temperature dependence of impact ionization with an adjusted model. Up to the initial current plateau of approximately 100 mA, the current waveforms are perfectly identical. This demonstrates that the local temperature rise is completely negligible in this early phase, and therefore, the device physics and transient behaviors in this specific regime are fundamentally independent of self-heating effects. The impact of self-heating becomes significant only in the later phase (beyond 500 mA). It is a well-established physical property that the impact ionization rate is heavily suppressed at elevated temperatures. In the default simulation where the standard temperature dependence is applied, the current prematurely peaks at 500 mA and subsequently decays, with the maximum temperature stalling at approximately 800 K due to this thermal suppression. It is important to note that the massive generation of intrinsic carriers, which ultimately leads to thermal runaway does not occur unless the local temperature reaches a sufficiently high critical threshold. In our TCAD framework, the device never reaches this critical temperature without simultaneously enhancing the impact ionization rate (by scaling the effective electric field by a factor of 1.41) and intentionally adjusting its temperature dependence to

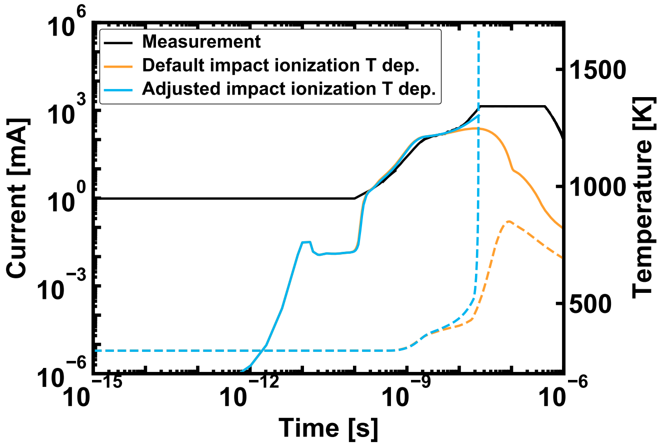

Fig. 12. Comparison of the transient current and maximum device temperature with and without the thermal calculation. Up to the initial current plateau of approximately 100 mA, the current waveforms are perfectly identical, demonstrating that the influence of self-heating is negligible in this early phase. In contrast, in the region beyond 500 mA, the model that disables the thermal suppression of the impact ionization rate ("Adjusted impact ionization T dependence") successfully reproduces the rapid current surge observed in the measurement, with the temperature reaching the melting point of silicon.

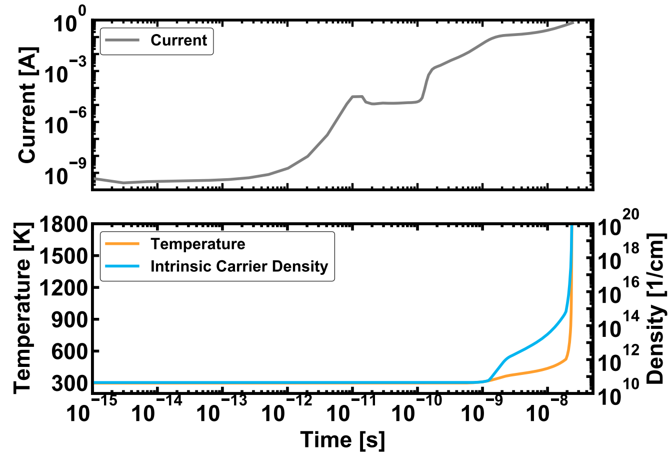

Fig. 13. Comparison of the simulated transient current and maximum device temperature using the default and adjusted temperature dependence models for impact ionization. The intrinsic carrier density exhibits an exponential surge precisely concurrent with the rapid rise in local temperature. This strongly indicates that thermally generated intrinsic carriers overwhelm the background doping concentration, driving the true thermal runaway mode that ultimately leads to device destruction.

prevent thermal degradation. Conversely, when the thermal degradation of impact ionization is intentionally disabled, the simulation successfully reproduces the explosive current waveform beyond 500 mA, allowing the local temperature to reach the melting point of silicon.

This catastrophic current surge beyond 500 mA is no longer sustained by impact ionization, but is instead driven by the massive generation of intrinsic carriers. This mechanism is strongly corroborated by Fig. 13, which illustrates the transient evolution of the intrinsic carrier density. The intrinsic carrier concentration exhibits a sharp, exponential surge precisely concurrent with the rapid temperature spike. This clearly indicates the transition into a true thermal runaway mode, where thermally generated intrinsic carriers overwhelm the background doping concentration, ultimately leading to device destruction. Because our detailed mechanistic investigation in this study is strictly confined to the early isothermal phase ($<$ 100 mA) substantially before the onset of this thermal runaway mode, the omission of the thermal calculation is physically valid and completely justified for evaluating the initial current amplification mechanism.

C. Physical Basis of Parameter Adjustments for SEB Reproduction

1) Statistical Nature of Impact Ionization: We additionally performed a simplified Monte Carlo simulation to investigate the stochastic nature of impact ionization. In this approach, the motion of individual carriers in a reverse bias diode was tracked within the depletion region, using the model given in [28]. The simulated diode's state was defined by the electric field distribution corresponding to the operating bias condition used in the SEB experiments. A hole was placed near the edge of the depletion layer, and its motion was discretized into finite steps. At each step, the probability of impact ionization was evaluated according to the field strength. New carriers were

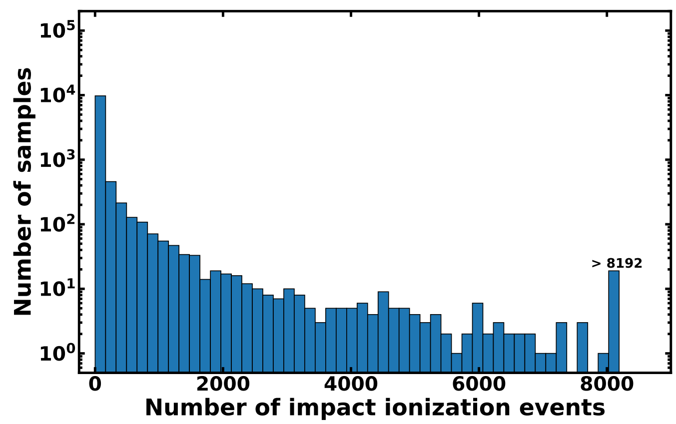

(a) Nominal model (van Overstraeten-de Man avalanche model, parameter set with scaling factor = 1.0).

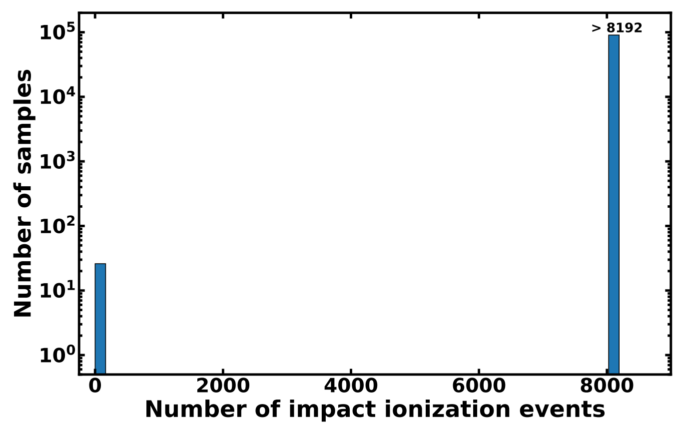

(b) Adjusted model (van Overstraeten-de Man with parameter b adjusted, equivalent to evaluating ionization at an effective electric field increased by a factor of 1.41).

Fig. 14. Histograms of Monte Carlo simulation results for impact ionization event counts in a reverse bias diode, obtained from 10^5 independent trials under two parameter sets.

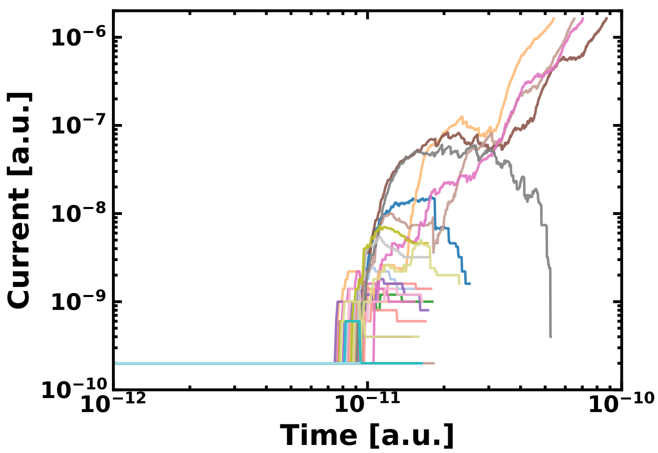

Fig. 15. The time evolution of the current by impact ionization obtained from 10^5 Monte Carlo simulation trials under the default van Overstraeten-de Man model. The graph displays 20% of the samples for clarity.

created according to this probability. This process was repeated until either no carriers remained in the depletion region or the number of ionization events exceeded a predefined threshold ($>$ 8192), which was defined as breakdown. A total of 10^5 independent trials were performed to obtain statistically meaningful distributions. Simulation using the default van Overstraeten-de Man model in Fig. 14a showed that only a very small fraction (0.017%) of samples developed into breakdown. In contrast, simulation using the adjusted van Overstraeten-de Man model, where the ionization coefficient was evaluated at an effective electric field 1.41 times larger (Fig. 14b), showed that around 90% of the samples developed into breakdown. This supports the interpretation that SEB arises only when rare statistical upward fluctuations in the number of impact ionization events occur. The 1.41 adjustment thus corresponds to the statistical upper tail of the ionization distribution, bridging deterministic TCAD with stochastic carrier dynamics. Physically, this adjustment lowers the effective critical electric field, representing rare but plausible upward fluctuations in avalanche multiplication.

Fig. 15 shows the time evolution of the current by impact ionization under the default condition. Most trials quickly terminated after a few ionization events, whereas a very small number developed into continuous impact ionization chains that progressed without suppression. This result also demonstrates both the intrinsic variability of impact ionization and the extreme rarity of sequences that accumulate enough events to cross the breakdown threshold, providing the microscopic origin of avalanche multiplication leading to SEB.

The physical basis for this stochastic variability lies in the relationship between the ionization mean free path and the device dimensions. Our Monte Carlo analysis indicates that the mean free path for impact ionization is distributed around 1.0 to 2.0 μm, peaking at approximately 1.5 μm. Since this mean free path is highly comparable to the effective length of the high-electric-field region near the p-n junction in the tested power device (which is on the order of several micrometers), each carrier undergoes only a very limited number of ionizing collisions. This makes the avalanche process inherently discrete and sensitive to individual scattering events, naturally leading to the extreme rarity of breakdown sequences observed in Fig. 14.

For quantitative comparison with measurements, the Monte Carlo simulation results were converted into failure in time (FIT) values, normalized to the experimentally measured FIT as unity. Using the default van Overstraeten-de Man model, the normalized FIT was approximately 7×10^{-3} [a.u.], more than two orders of magnitude smaller than the experimental reference. This severe underestimation demonstrates that most simulated events do not reach the breakdown threshold, consistent with the interpretation that SEB is triggered only by extremely rare statistical fluctuations. Thus, the default simulation serves as direct supporting evidence that SEB is fundamentally a rare-event.

2) Effective LET Scaling: To physically justify the application of the LET scaling factor used in our TCAD simulations, we must address a fundamental limitation in the standard TCAD heavy-ion model. In our default model, the generated carriers are assumed to possess zero initial energy (0 eV). However, in actual neutron-induced nuclear spallation reactions, the resulting secondary ions impart significant initial energy to the generated carriers. We hypothesize that this lack of initial energy represents the missing physical mechanism critical for accurately reproducing SEB failure dynamics in standard TCAD setups. To quantitatively evaluate the impact of this missing initial energy, we performed detailed Full-Band Monte Carlo (FBMC) simulations [29]. The FBMC model considered five conduction bands and four valence bands in silicon, incorporating phonon scattering and impact ionization. Carrier transport was simulated using a frozen-field approach within the depletion region of a one-sided p-n junction. The simulation was terminated, and an avalanche event was recorded, when the total number of carriers exceeded 128. To clarify the discrepancy between the standard TCAD model and realistic physical phenomena, we compared three initial conditions:

(a) 1 electron at 0 eV: Equivalent to the conventional TCAD setup.
(b) 1 electron at 10.8 eV: Equivalent to the realistic high-energy state immediately after a spallation reaction.
(c) 3 electrons at 0 eV: Equivalent to our proposed compensation method (LET scaling), where the initial charge amount is increased instead of initial energy.

The physical equivalence between conditions (b) and (c) is derived from the principle of energy conservation. Since the average energy required to generate one electron-hole pair in silicon is approximately 3.6 eV, a single 10.8 eV electron theoretically possesses the potential to generate three pairs. Thus, conditions (b) and (c) are physically equivalent in terms of the total energy introduced into the system. It is important to note that while the TCAD setup correctly calculates the macroscopic number of carriers using the pair creation energy (3.6 eV), it fails to account for their initial high-energy state by artificially depositing them at thermal equilibrium (0 eV). In actual spallation reactions, however, these generated carriers retain significant kinetic energy as ”hot carriers” that can

TABLE II
COMPARISON OF AVALANCHE PROBABILITY UNDER DIFFERENT INITIAL CONDITIONS IN FBMC SIMULATION

Case	Initial Condition	Trials	Avalanche probability
(a)	1 e^- @ 0 eV	339	0.180
(b)	1 e^- @ 10.8 eV	154	0.396
(c)	3 e^- @ 0 eV	163	0.356

immediately trigger impact ionization. The FBMC simulation results are summarized in Table II.

The default TCAD condition (a) yielded an avalanche probability of only 18.0%, which is less than half of the 39.6% observed for the realistic high-energy condition (b). This discrepancy arises because carriers with 0 eV initial energy require longer travel distances to be accelerated by the electric field and reach the impact ionization threshold, thereby critically delaying the onset of avalanche multiplication. This quantitatively demonstrates that the default TCAD model severely underestimates the SEB probability due to the neglect of initial energy. Crucially, under our proposed compensation method (c), the avalanche probability recovered to 35.6%, reaching approximately 90% of that under the realistic condition (b). This confirms that even in the absence of initial energy, increasing the initial carrier count to an energy-equivalent amount can successfully guarantee a realistic avalanche probability.

Regarding the multiplication factor of 30, a physically quantitative mechanism that fully explains this specific value has not been identified at this time. As evaluated by energy conservation (3.6 eV per electron-hole pair), the direct physical increase in carrier generation would be limited. However, the issue of the initial energy of secondary ions is considered to be one of the factors necessitating this factor of 30. In reality, generated carriers possess significant initial kinetic energy, inducing autonomous, ultra-fast transient avalanche multiplication in the picosecond regime immediately after the nuclear reaction. Since standard TCAD tools assuming a 0 eV initial energy lack the physics to calculate this non-equilibrium transient phase, mapping the highly dense carrier state after this initial multiplication onto the initial condition ($t = 0$) is considered as a potential factor requiring this large effective scaling, although fully quantifying this multi-scale mechanism remains a subject for future work.

D. Cross-Sectional Analysis of SEB-Induced Damage Region

To investigate the physical consequences of SEB, the Optical Beam Induced Resistance Change (OBIRCH) method [30] was employed to identify the failure sites. Cross-sectional observations were carried out using electron microscopy. Fig. 16 compares the damage regions observed at 1000 V reverse bias with and without parallel capacitance.

Both conditions resulted in permanent FRD failure. When no parallel capacitance was added (Fig. 16a), the damaged region remained localized. Aluminum electrode penetration was shallow, and silicon melting as well as thermally induced cracks were limited in extent. In contrast, when 2 nF parallel capacitance was included (Fig. 16b), the damaged region expanded both vertically into the drift region and laterally. Severe

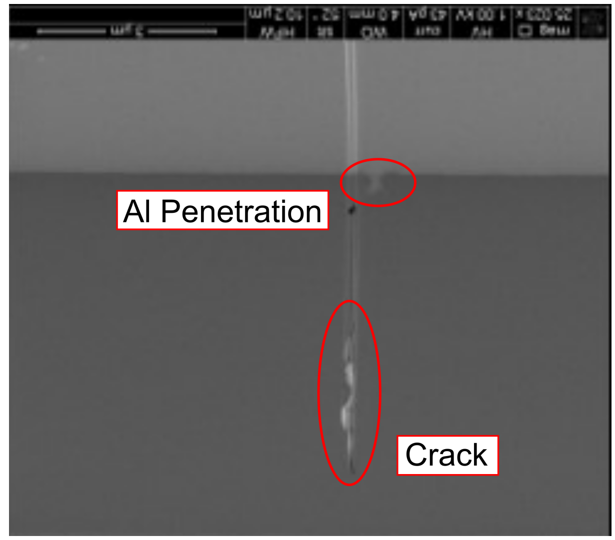

(a) Without capacitance.

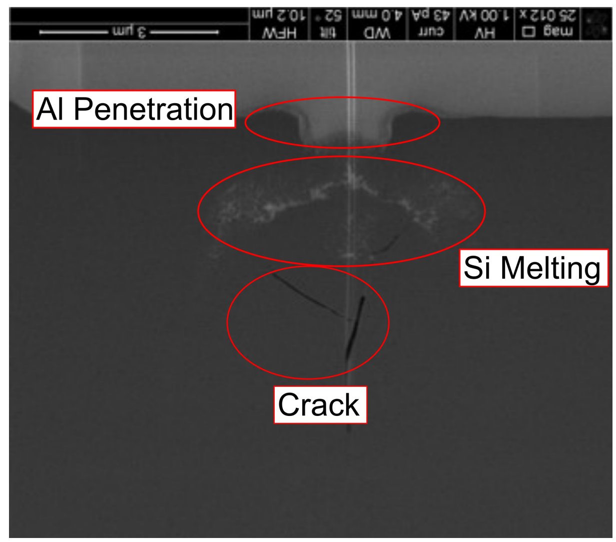

(b) With 2 nF capacitance.

Fig. 16. Cross-sectional damage regions of the FRD under a reverse bias of 1000 V.

aluminum intrusion, large-scale silicon melting, and multiple thermal stress-induced cracks were observed. These findings clearly demonstrate that the presence of parallel capacitance significantly enlarges the damaged region and enhances the severity of SEB-induced burnout. Reverse resistance measurements supported these observations. An undamaged device exhibited resistance values on the order of several GΩ. After SEB, the resistance degraded to tens of MΩ without capacitance, and further dropped to only a few MΩ with capacitance. The pronounced reduction in the latter case is attributed to the extensive aluminum penetration observed in Fig. 16b.

Eliminating the parallel capacitance suppresses thermal melting, enabling the identification of the minimum failure current and providing clearer insights into the intrinsic SEB trigger mechanism. Conversely, including capacitance emulates surge conditions in practical circuits, which is essential for assessing device reliability under realistic environments.

Therefore, both conditions provide complementary insights: capacitance-free observations reveal the fundamental mechanisms, whereas capacitance-included cases reflect application-level reliability concerns. These findings are consistent with earlier reports of catastrophic aluminum penetration and melting damaged regions in silicon power diodes under heavy-ion irradiation [12], reinforcing the crucial role of parasitic capacitance in accelerating burnout progression.

V. Conclusion

This work investigated SEB in a 1200V Si FRD through neutron irradiation experiments and device simulations. Transient current and voltage measurements clarified that failure is not set by the initial peak alone but develops when avalanche multiplication sustains the current. Statistical measurements at 930 V without external capacitance showed that only one in ten irradiation events lead to burnout, providing direct experimental evidence that SEB is governed by stochastic upward fluctuations in impact ionization rather than by a deterministic threshold.

To interpret these findings, we coupled particle transport simulations with device modeling. PHITS simulations identified worst-case secondary-ion conditions, from which heavy-ion parameters for TCAD excitation were extracted. Default Sentaurus simulations using the van Overstraeten-de Man avalanche model underestimated the peak and persistence of SEB current, failing to reproduce measurements. By contrast, two physically motivated adjustments enabled quantitative reproduction: adjusting the model parameter b so that the ionization coefficient is evaluated at an effective electric field 1.41 times larger, effectively representing the statistical upper tail of avalanche multiplication; and second, applying an effective LET scaling factor of 30. While fully quantifying the exact factor of 30 remains a subject for future work, the issue of initial energy is considered one of the potential factors necessitating this large scaling. Standard TCAD assumes a 0 eV initial energy and lacks the physics to calculate the non-equilibrium transient phase; therefore, mapping the highly dense carrier state after the fast transient multiplication onto the initial condition ($t = 0$) phenomenologically compensates for this tool limitation. With these adjustments, the simulated current waveforms matched the measured rise and sustained growth under neutron irradiation.

SEB in power diodes arises from rare and extreme ionization events that cannot be captured by deterministic models alone. The combination of experimental statistics and physics-based parameter adjustments establishes a practical methodology for reproducing SEB currents and provides new insight into the stochastic nature of neutron-induced burnout.

VI. Acknowledgment

The authors thank the Research Center for Nuclear Physics (RCNP), Osaka University and the Gunma University Heavy Ion Medical Center (GHMC) for supporting the neutron experiments. This work was supported through the activities of d-lab. VDEC, The University of Tokyo, in collaboration with NIHON SYNOPSYS G.K.

References

[1] A. Sengupta *et al.*, "LET and voltage dependence of single-event burnout and single-event leakage current in high-voltage SiC power devices," *IEEE Trans. Nucl. Sci.*, vol. 71, no. 4, pp. 809–815, Apr. 2024.

[2] L. Scheick, G. Allen, L. Edmonds, R. Schaefer, and R. Menke, "Observation of single-event burnout during inductive switching," *IEEE Trans. Nucl. Sci.*, vol. 65, no. 2, pp. 719–723, Feb. 2018.

[3] A. F. Witulski *et al.*, "Single-event burnout of SiC junction barrier schottky diode high-voltage power devices," *IEEE Trans. Nucl. Sci.*, vol. 65, no. 1, pp. 256–261, Jan. 2018.

[4] D. L. Oberg and J. L. Wert, "First nondestructive measurements of power MOSFET single event burnout cross sections," *IEEE Trans. Nucl. Sci.*, vol. 34, no. 6, pp. 1736–1741, Dec. 1987.

[5] J. Titus, Y.-S. Su, M. Savage, R. Mickevicius, and C. Wheatley, "Simulation study of single-event gate rupture using radiation-hardened stripe cell power MOSFET structures," *IEEE Trans. Nucl. Sci.*, vol. 50, no. 6, pp. 2256–2264, Dec. 2003.

[6] A. F. Witulski *et al.*, "Single-event burnout mechanisms in SiC power MOSFETs," *IEEE Trans. Nucl. Sci.*, vol. 65, no. 8, pp. 1951–1955, Aug. 2018.

[7] D. R. Ball *et al.*, "Ion-induced energy pulse mechanism for single-event burnout in high-voltage SiC power MOSFETs and junction barrier schottky diodes," *IEEE Trans. Nucl. Sci.*, vol. 67, no. 1, pp. 22–28, Jan. 2020.

[8] G. Johnson, J. Palau, C. Dachs, K. Galloway, and R. Schrimpf, "A review of the techniques used for modeling single-event effects in power MOSFETs," *IEEE Trans. Nucl. Sci.*, vol. 43, no. 2, pp. 546–560, Apr. 1996.

[9] A. Albadri, R. Schrimpf, K. Galloway, and D. Walker, "Single event burnout in power diodes: Mechanisms and models," *Microelectron. Rel.*, vol. 46, no. 2, pp. 317–325, Feb. 2006.

[10] T. Shoji, S. Nishida, and K. Hamada, "Triggering mechanism for neutron induced single-event burnout in power devices," *Jpn. J. Appl. Phys.*, vol. 52, no. 4S, Apr. 2013, Art. no. 04CP06.

[11] O. Musseau *et al.*, "Medium-energy heavy-ion single-event-burnout imaging of power MOSFETs," *IEEE Trans. Nucl. Sci.*, vol. 46, no. 6, pp. 1415–1420, Dec. 1999.

[12] T. Shoji, S. Nishida, K. Hamada, and H. Tadano, "Observation and analysis of neutron-induced single-event burnout in silicon power diodes," *IEEE Trans. Power Electron.*, vol. 30, no. 5, pp. 2474–2480, May 2015.

[13] S. Kuboyama, C. Kamezawa, N. Ikeda, T. Hirao, and H. Ohyama, "Anomalous charge collection in silicon carbide schottky barrier diodes and resulting permanent damage and single-event burnout," *IEEE Trans. Nucl. Sci.*, vol. 53, no. 6, pp. 3343–3348, Dec. 2006.

[14] S. Islam *et al.*, "Single-event burnout in vertical β-Ga_2O_3 diodes with Pt/PtO_x schottky contacts and high-k field-plate dielectrics," *IEEE Trans. Nucl. Sci.*, vol. 71, no. 4, pp. 515–521, Apr. 2024.

[15] S. Kuboyama, S. Matsuda, T. Kanno, and T. Ishii, "Mechanism for single-event burnout of power MOSFETs and its characterization technique," *IEEE Trans. Nucl. Sci.*, vol. 39, no. 6, pp. 1698–1703, Dec. 1992.

[16] "MIL-STD-750E," Test method standard - Test methods for semiconductor devices, 2006.

[17] T. A. Fischer, "Heavy-ion-induced, gate-rupture in power MOSFETs," *IEEE Trans. Nucl. Sci.*, vol. 34, no. 6, pp. 1786–1791, Dec. 1987.

[18] C. W. Slayman, "Theoretical correlation of broad spectrum neutron sources for accelerated soft error testing," *IEEE Trans. Nucl. Sci.*, vol. 57, no. 6, pp. 3163–3168, Dec. 2010.

[19] T. Ohno *et al.*, "Carbon ion radiotherapy at the gunma university heavy ion medical center: New facility set-up," *Cancers*, vol. 3, no. 4, pp. 4046–4060, Oct. 2011.

[20] M. Sakai *et al.*, "Soft error measurement for carbon ion radiotherapy," *Nucl. Instrum. Methods Phys. Res. Sect. B*, vol. 553, Aug. 2024, Art. no. 165384.

[21] R. Nakajima *et al.*, "A measurement method for neutron-induced soft-error rates in terrestrial applications using a clinical carbon beam," *IEEE Trans. Nucl. Sci.*, vol. 72, no. 10, pp. 3235–3246, Oct. 2025.

[22] E. Normand, "Extensions of the burst generation rate method for wider application to proton/neutron-induced single event effects," *IEEE Trans. Nucl. Sci.*, vol. 45, no. 6, pp. 2904–2914, Dec. 1998.

[23] *Measurement and Reporting of Alpha Particle and Terrestrial Cosmic Ray-Induced Soft Errors in Semiconductor Devices*, Standard JEDEC JESD89B, 2021.

[24] T. Sato *et al.*, "Recent improvements of the particle and heavy ion transport code system – PHITS version 3.33," *J. Nucl. Sci. Technol.*, vol. 61, no. 1, pp. 127–135, Jan. 2024.

[25] J. Ziegler, "Terrestrial cosmic rays," *IBM J. Res. Develop.*, vol. 40, pp. 19–40, Jan. 1996.

[26] A. G. Chynoweth, "Ionization rates for electrons and holes in silicon," *Phys. Rev.*, vol. 109, pp. 1537–1540, Mar. 1958.

[27] R. Van Overstraeten and H. De Man, "Measurement of the ionization rates in diffused silicon p-n junctions," *Solid-State Electron.*, vol. 13, no. 5, pp. 583–608, May 1970.

[28] R. Klanner and J. Schwandt, "SiPM understanding using simple geiger-breakdown simulations," *Nucl. Instrum. Methods in Phys. Res. Sect. A*, vol. 1062, May 2024, Art. no. 169233.

[29] T. Kunikiyo *et al.*, "A Monte Carlo simulation of anisotropic electron transport in silicon including full band structure and anisotropic impact - ionization model," *J. Appl. Phys.*, vol. 75, no. 1, pp. 297–312, Jan. 1994.

[30] K. Nikawa, "Optical beam induced resistance change (OBIRCH): overview and recent results," in *Proc. The 16th Annu. Meeting of the IEEE Lasers and Electro-Optics Soc.*, vol. 2, Tucson, AZ, USA, Jan. 2003, pp. 742–743.